Graphical Abstract

Global optimisation approach for designing high-efficiency piezoelectric beam-based energy harvesting devices

Daniil Yurchenko, Lucas Queiroz Machado, Junlei Wang, Chris Bowen, Suleiman Sharkh, Mohamed Moshrefi-Torbati, Dimitri V. Val

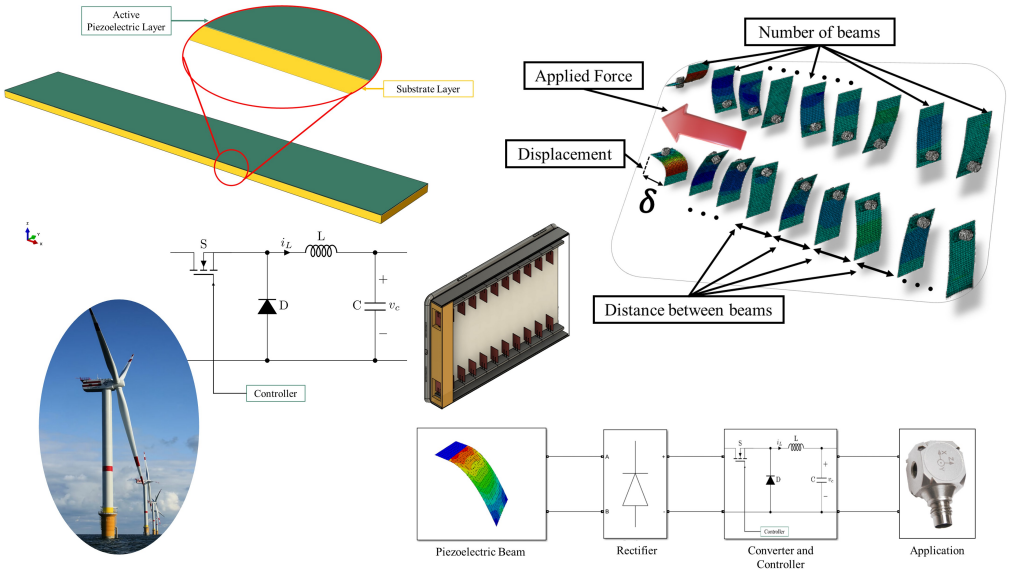

Figure 1: Overview

Global optimisation approach for designing high-efficiency piezoelectric beam-based energy harvesting devices

Daniil Yurchenko[a], Lucas Queiroz Machado[a], Junlei Wang[b,*], Chris Bowen[c], Suleiman Sharkh[d], Mohamed Moshrefi-Torbati[d], Dimitri V. Val[e]

[a]*IMPEE, Heriot-Watt University, Edinburgh, UK.*
[b]*School of Mechanical and Power Engineering, Zhengzhou University, Zhengzhou, China.*
[c]*Department of Mechanical Engineering, University of Bath, Bath, UK*
[d]*Department of Mechanical Engineering, University of Southampton, Southampton, UK.*
[e]*IIE, Heriot-Watt University, Edinburgh, UK.*

Abstract

The paper proposes a novel methodology for developing high-power energy harvesting gravity-based devices using an array of piezoelectric beams for wind energy applications. The methodology incorporates a global multidimensional constrained optimisation algorithm, which accounts for the physical size of the device, the physical, geometrical and electrical properties of the piezoelectric beams, and the power management circuit to increase the device's efficiency. As the beams are plucked sequentially, they vibrate out-of-phase, which consequently leads to charge cancellation issues. The paper proposes and incorporates an electrical circuit design to avoid such problems, being able to further increase the efficiency of the device by 35% when compared against the output from the standard energy harvesting (SEH) circuit with independent rectifiers. The proposed optimisation methodology is applied to the devices utilizing flexible polyvinylidene fluoride beams. The developed dynamic numerical model of the beams' vibration is validated using the experimental results and the results of a Finite Element Analysis. To study the electro-mechanical coupling of the beams, an electric circuit and the power management circuit are created and modeled in Matlab/Simulink software. The optimised device deliveres 6 to 17 times higher energy output compared to the unoptimised device. The performance of this device was also compared to that of the device with much stiffer $LiNbO_3$ beams [1] to demonstrate the direct

*Corresponding author email: jlwang@zzu.edu.cn

applicability of such devices to power sensors and transmitter units for structural monitoring of wind turbine blades. It has been demonstrated that the $LiNbO_3$-beam device yields an energy output with one order of magnitude higher. The applied optimisation methodology enabled a 0.057x0.01x2m dimension device to produce a power output in the range from 0.5 to 1 W depending on the blades' speed, resulting in 1.06 mW/cm^3 power density of the device.

Keywords: Energy Harvesting, Free Vibrations, Piezoelectric, Polyvinylidene Fluoride beams, $LiNbO_3$, Rectification Circuit, optimisation

1. Introduction

In recent years energy harvesting (EH) from ambient vibrations has become a well-defined branch of science with efforts focused on the development of efficient and reliable devices, which can scavenge mechanical energy and convert it into electrical energy. Since vibrations often occur in civil and mechanical systems, they are deemed to be one of the available sources of energy in a variety of applications. The latter include human activities, structural vibrations in buildings and bridges, vibrations in machines and mechanisms in railway, automotive, aerospace and renewable energy sectors. It should be stressed that vibrations in man-built systems are typically treated as an adverse effect, which is mitigated whenever possible, thus, the level of vibrations available for EH is relatively small. In general, a major motivation behind the EH development was to create an application-oriented device, which could recharge a battery powering a solitary sensor or sensor networks, such as Body Sensors Network (BSNs), Wireless Sensors Networks (WSNs), the Internet of Things (IoT) and the Industrial Internet of Things (IIoTs) [2, 3]. Indeed, wireless sensors require power to operate and transmit information, therefore such sensors require a power supply, e.g., batteries. Although a significant progress has been achieved in the development and miniaturisation of batteries, they have to be replaced regularly. Rechargeable batteries can withstand hundreds and even thousands of recharging cycles, however, it is well-known that their capacity and voltage drop over time and, eventually, they will need to be replaced and disposed as well.

Despite a large number of publications in the area of EH from ambient vibrations, few practical devices have been developed and even fewer have been commercialised or are actually used today. There are a number of reasons for a relatively slow proliferation of such EH devices, among which are: a low energy density, a narrow operating bandwidth, nonlinear scaling effects, low level of

absolute generated power due to a low level of structural vibrations, and fatigue issues when piezoelectric beams operate at their resonance frequencies. Typically, a vibration EH device takes advantage of one of the four vibration energy conversion methods [4, 5], namely piezoelectric (PE) [6, 7], electromagnetic [8], electrostatic [9, 10], and triboelectric [8, 11]. These types of devices comprise two parts: a mechanical system for power take off and a transduction mechanism for energy conversion. The devices utilizing piezoelectric transduction, are able to work in the tension/compression or bending mode; the latter is usually achieved using a cantilever beam with a single or multiple layers of PE material.

The wide proliferation of PE cantilever-beam devices comes from their relatively simple implementation, straightforward miniaturisation to micro- and nanoscale [12], and the ability to apply an excitation to the fixed or free end of the beam. A classical PE EH cantilever-beam device has a narrow bandwidth and a high natural frequency, in order of hundreds of hertz. Such a frequency is hard to match in the vast majority of practical applications to make the beam response high, although there are some exceptions in MEMS and mesoscale devices [7]. Nevertheless, the PE beam-based devices have been proposed to be used for harvesting wind energy [13, 14], energy from oscillatory and rotational motion [15, 16, 17], as well as in devices with nonlinear damping and/or stiffness [18, 19, 7, 20]. When a cantilever beam is excited outside of its bandwidth or the excitation is relatively wide band its response amplitude is low leading to low power output. It is possible to decrease the cantilever beam's natural frequency by adding a lumped mass to its tip (free-end), however this tuning has obviously practical, geometrical and physical limitations. Another way to address the bandwidth problem is by adopting mechanical frequency-up (MFU) conversion, as will be explained later.

In the last twenty years it has been learned that linear small-size PE harvesters consisting of a single PE beam are not capable of generating the power required for consistent operation of a wireless sensor, moreover, it is often insufficient for recharging a battery. Thus, researchers have recently examined other options for improving the mechanical element of harvesters, considering smooth and non-smooth mechanically nonlinear systems, systems with multiple equilibria, as well as systems with multiple beams connected together by springs or connected to a common base [21, 22, 23]. All these ideas aimed to overcome the challenges that the linear systems face. For example, low excitation frequency can be used to generate high frequency oscillations using frequency-up conversion. This usually involves two components: first, a (non) resonant primary element which responds to low frequency input excitation, and, second, a harvester (a beam vibrating at

a higher frequency), which responds to the primary element. This is mainly accomplished via impact interaction [24, 25, 26, 27], contact plucking [28, 29] and magnetic contactless plucking [30, 31, 32]. In all these cases, the primary element is used to impose an initial deflection on the PE beam. Once the interaction between them ceases, the harvester is let to freely vibrate due to imposed initial displacement at its fundamental bending mode. This is known to improve the power output of the harvester when bandwidth is an issue [28]. In this context Yipeng et al. [33] presented a harvester whose operational frequency was six times higher than that of the input and could be applied to oscillatory sources with frequencies in the range of 1-5 Hz. Gu and Livermore [34] presented an impact-driven harvester, whose power density was increased about 13 times when compared to its conventional counterpart.

Typically, the frequency-up conversion approach implies a certain layout of the PE beams in a comb-like structure, where the beams face each other through their width. There are two factors that should be emphasised when such an array of PE beams with frequency-up conversion is involved. First, free vibration EH has been investigated much less than forced vibration EH. There are a number of issues associated with free vibrations, for instance, decaying oscillations. The latter generate decaying signal that cannot be treated as a DC, even after rectification, especially when there are several PE beams connected electrically into a system. Second, combining PE beams into an array raises a number of challenges, some of which remain unresolved. For instance, for a given volume of an EH device, what is the optimal number of PE beams; what are the optimal shapes and sizes of the PE beams; what are the ways to excite PE beams; how the multiple beams should be connected electrically, and how the power should be managed? Some of these questions have been addressed separately in a number of papers, which discuss a PE beam's shape and cross-section optimisation [35, 36], electrical circuit optimisation [37, 38]. When no physical constraints are imposed on the overall device size, obviously the beam's parameters should match the excitation in one way or another, when the device is subjected to a harmonic excitation. When the device size is subjected to a physical constraint its performance is dictated by the number of PE beams, their thickness, that can be fitted within the device, their tip displacement (which has to be taken into account not only to avoid excessive stress, but also potential collisions between the beams' tips), stiffness, all of which influence the device power output. Moreover, all these parameters are nonlinearly interconnected to each other, so that an optimal performance of a single beam may not necessarily lead to the best performance of multiple electrically connected PE beams within the device. Thus, it is important to develop a method-

ology, which can be used for optimisation of constrained PE-beams type devices for EH from vibration, and to the best of the authors' knowledge there is no such a framework. An effort to take into account the device physical constraints was undertaken in [39], where an energy harvesting gravity-based device was developed for e-gadgets. However, the proposed algorithm lacked some steps and was not systematically presented.

This paper proposes a new general global multidimensional optimisation algorithm for optimising the performance of a PE multi-beam gravity-based device for EH in wind applications for powering wireless sensors and data transmission. While arrays adopting plucking mechanisms have been addressed in the literature [29, 40] this device adopts a piezoelectric array structure along with a plucking mechanism to illustrate how a new algorithm improves the response of well-known energy harvesting designs. Section 2 describes the framework of the proposed optimisation algorithm. Then the concept is introduced using flexible polyvinylidene fluoride beams; the beam's finite element model is built and validated against experimental data, and the optimisation algorithm is described, which are presented in Section 3. Section 4 presents the numerical results based on the developed numerical model of dynamical response of a PE cantilever beam with or without a tip-mass. Then, the surrogate optimisation results are presented and compared to the performance of the device without optimisation. Then the performance of the device with $LiNbO_3$ is assessed for health monitoring of wind turbine blades. The conclusions are provided in Section 5.

2. Proposed optimisation Methodology

The design is a function of constants, variables and constraints, which depends on the application. In this context, the constants are predefined values of the model, which are not subjected to the optimisation routine, such as the PE material constants, and device's length and width. The variables are the parameters, which will be optimised within the optimisation process, e.g., the size and thickness of the PE beam's substrate, which influence the beam's stiffness and natural frequency. The constraints can be expressed in terms of absolute values or inequalities between mathematical expressions. Table 1 presents all the parameters related to the optimisation process and classify them into constants, variables, and constraints. This table does not contain the parameters of a buck-boost DC-DC converter, which can also be optimised through the proposed algorithm.

Figure 2 demonstrates the flowchart of the proposed design optimisation framework. Selecting an appropriate optimisation algorithm is a critical step within this

Table 1: Parameters related to the design of the energy harvester classified into constants, variables and constraints

Constants	Variables	Constraints
Device Dimensions L_d, W_d, t_d	Beam's Tip Displacement δ	Maximum Beams Stress σ_{max}
PE Mechanical Constants ρ_p, Y_p	Substrate Thickness t_s	Maximum Carriage Length L_{Mmax}
PE Substrate constants ρ_s, Y_s	Piezoelectric Thickness t_p	Maximum Carriage mass M_{max}
Beams' Length and Width l_b, w_b	Number of Beams, Pins and Beams Between Pins n_b, n_p, n_{bbp}	Max/Min Tip Displacement $\delta_{max}, \delta_{min}$
Carriage Width W_c	Carriage Mass, Length, Thickness M_c, L_c, t_c	
PE Constant d_{ij}, ε	Optimal Resistance, Beam Capacitance R_{opt} , C_p	Maximum Ouput Voltage V_{max}

framework. Priority should be given to a global multidimensional optimisation algorithm capable of dealing with computationally inefficient, time-consuming objective functions, preferably the one that accepts defining finite bounds on its variables and is independent of initial estimations. The device's topology and the beam's excitation input are known in advance and are modelled using a set of governing differential equations of motion. There are several possible scenarios, which have to be taken into account, including the options when all the PE beams are excited simultaneously, separately, or a combination of both. The algorithm carries out the optimisation by maximising the power output of the entire device for multiple sets of parameters. The algorithm proposes an optimisation process at the beam level as well as at the device level. At the beam level, an electromechanical model of the PE beam is used to optimise its performance under the imposed constraints. It includes the beam's shape and its cross-section shape, its dimensions and the properties of both the substrate and PE layers. The electrical properties of each beam, including the beam's connection to the rectification bridge and other intermediate components before connecting to other beams are optimised at this level.

Obviously, optimisation at the beam level influences the device performance and vice versa. Next, the mechanical parameters at the device level are optimised, where the total number of the beams, the tip displacement of each beam, the mass of the system and the magnitude and frequency of the excitations are taken into account. As can be seen, the excitation's properties input the system at the de-

vice level, since typically the entire device is subject to the excitation, not a single beam. For example, it is easy to see that thicker beams will restrict the total number of the beams within a given device size. Since the beams are not supposed to touch each other, the tip displacement of each beam will impose an additional constraint on the minimum free space available between each beam, again influencing the total number of the beams. On the electrical side, multiple beams pose a problem, especially in the case when they generate decaying signals. There

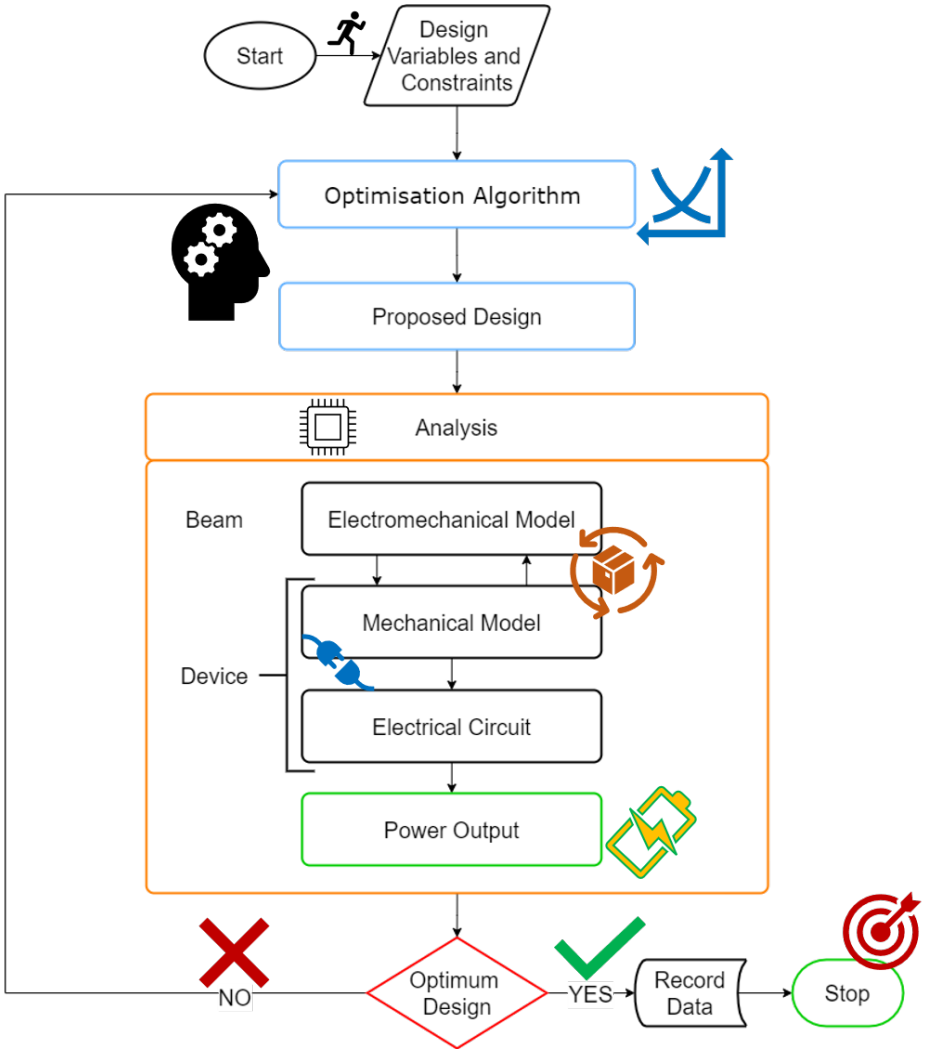

Figure 2: Design optimisation flowchart

are several well-known options, including the Standard Energy Harvesting (SEH), the Voltage Doubling Rectifier (VDR), and the series and parallel Synchronized Switch Harvesting on Inductor (SSHI) interfaces, which in conjunction with DC-DC converters, such as the buck-boost, are employed in EH systems. However, they are greatly influenced by the capacitor voltage of the rectifier filter, as well as by the load impedance. For this reason and due to the decaying signal generated by the beam, not all energy generated by the beam will be stored. For instance, when the voltage across the filter capacitor rises above part of the decaying voltage generated by the PE beam, no charge is further stored in the capacitor and this energy is lost. This considerably decreases the efficiency of the system as potentially available energy is lost due to a poor power management circuit. The optimisation algorithm at this level will try to use different circuits to find the maximum energy output for the given number of beams and specified excitation parameters. As the output of this procedure, the total energy and power of the entire device are produced and recorded.

3. A gravity-based concept based on the proposed methodology

The methodology formulated above can be applied to any EH device with predefined volume, however, in this paper it will be applied to a concept of a gravity-based device that can be used to collect energy from its rocking motion, acceleration - deceleration motion or low speed rotation [17].

The proposed concept, aimed to capture this available energy, is designed as a cuboid (250.6x155.85x20 mm^3) with the in-plane sizes matching or be smaller than the size of a host structure, satisfying specified device's constraints. A mass, represented by a carriage, can move freely inside the device under the gravity force action, transforming its potential energy into kinetic energy, as shown in Figure 3. Figure 3a shows the proposed initial design of the device, where the carriage mass (yellow), have a plectrum attached to it. The plectrum attached to the carriage is the primary element used to impose an initial displacement to the beams as the carriage slides along the rails during this process. Figure 3b presents the FEM model output and illustrates the beams' vibration after the described process has taken place. Each beam is engaged once or several times depending on design during the carriage motion in one direction. To engage the beams, an overlap between the plectrum and the beam is required. The shorter the overlap, the easier the carriage can pluck the beams via the plectrum. Kathpalia et al. [28] presented a nonlinear plectrum-linear harvester framework that allows selecting the appropriate plectrum parameters to meet the required overlap conditions for

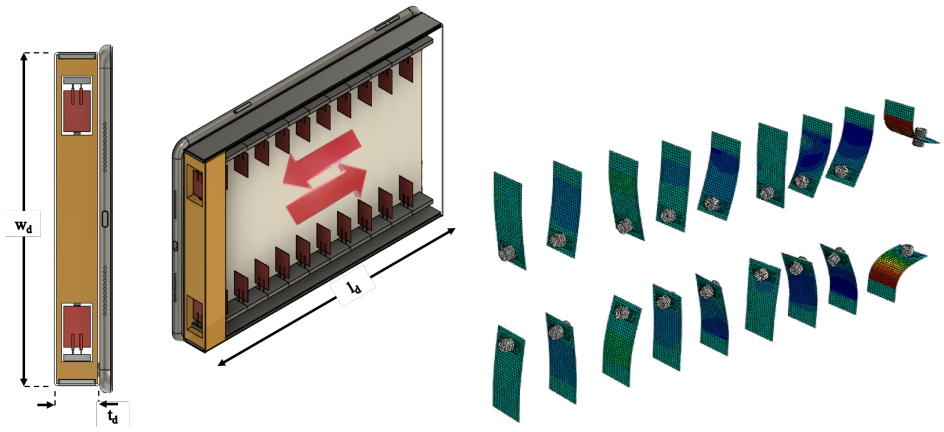

(a) (b)

Figure 3: Gravity-based concept with two-sided arrays of beams with tip mass (a) concept (b) finite element model.

the frequency up conversion. The characteristic feature of such a device is that the internal beams are excited sequentially and experience free decaying oscillations. The time interval between the excitation of consecutive beams depends on the mass speed relative to the beams, which, in turn, depends on the rocking motion of the device.

A few EH concepts have been proposed, where an array of PE beams was used [41, 21, 42]. The power output from an array of PE beams was analysed in [43] with no consideration to charge cancellation due to phase shift, which resulted in relative low power output. Later, the analytical modelling formulation for multiple PE beams connected to independent rectifiers was published in [38] where an attempt to eliminate charge cancellation. However, that solution does not prevent charge cancellation when the beams vibrate out-of-phase. While the rectification prevents negative and positive signals to cancel each other, it only allows the signal with the highest value to get through when all rectifiers are connected to the same point afterwards. Therefore, an effective power management to avoid charge cancellation has yet to be developed, and some discussion on this issue is provided later in Section 3.5.

Evidently, the gravity-based PE beams EH device's performance depends on the nonlinear interaction between several parameters. Since the harvester is application - oriented designed, it requires understanding the behaviour of the host structure, as well as understanding of the conversion mechanism. Key challenges and design principles are related to decisions about the amount of beams compos-

ing the array, the distance between them, the thickness of the substrate layer and the PE layer, the force needed to pluck them, and the displacement applied to each of them.

The methodology adopted to determine the best arrangement includes the implementation of a parametric algorithm, which numerically establishes the relationship between each leading parameter. This algorithm is then used in conjunction with an optimisation procedure.

Therefore, the proposed design is a result of a full geometric optimisation procedure applied to the parameters related to the device's performance, given required boundary conditions. The restrictions imposed are related to the width, length, and inclination angle of the target device and the maximum stress applied to the PE beam. Given these parameters, the optimisation procedure is carried out varying the thickness of the substrate as well as the thickness of the PE material. The number of PE beams within the array is defined by the space available from the length of the device, which is constant, the thickness of each PE beam, and the displacement applied to the beam, which may vary. For this reason, the displacement, along with the beam's thickness, is another parameter to be directly optimised. The stiffness of the beam is defined from its dimensions. Given the displacement and the stiffness of the beam, the necessary mass to pluck one or several beams is calculated for a given inclination angle. The power output depends on the frequency of operation, however the energy generated by the device as the mass moves from one side to the other is constant, i.e., depending on the operator, the mass can be moved at varying speeds changing the power output, but the energy produced per cycle does not change. Figure 2 presents the flowchart summarizing the steps taken to get to the proposed design.

3.1. Material

In this study, polyvinylidene fluoride (PVDF) beams are used due to their relatively low stiffness and flexibility, attributed to polymer based PE materials [44, 45]. Out of a range of flexible PE materials, the design will benefit the most from those with the highest g_{31} coefficient, because the bending mode EH is employed. Two types of PVDF-028K beams provided by Measurement Specialties, Inc. [46] with a $0.72 \times 10^{-3} kg$ tip-mass (LDTM) and without tip-mass (LDT0) were selected. The properties of these beams are shown in Table 2. The dimensions of the PVDF material, as indicated in Table 2, are relevant to the electrically active part of the PVDF, which is the area covered by the electrodes. For the mechanical modelling, the entire area of the PVDF material, which is the same as the

area of the Mylar, is taken into account. The tip-mass beam has the same characteristics as the massless one, but due to its tip-mass of $0.72 \times 10^{-3} kg$, which is 10 times greater than the beam mass, the beam's natural frequency is much lower.

3.2. Analytical Model

The actual beams, using in the experimental study, are shown in Figure 4a and composed of a single PE layer bonded to a substrate. The coupled distributed parameter electromechanical model adopted to predict the behaviour of the PE beam is expressed via two differential equations below [47]:

$$\begin{aligned} \frac{d^2\eta_r(t)}{dt^2} + 2\zeta\omega_r\frac{d\eta_r(t)}{dt} + \omega_r^2\eta_r(t) + \alpha_r v(t) = N(t), \\ C_p\frac{dv(t)}{dt} + \frac{v(t)}{R_l} = \sum_{r=1}^{\infty}\alpha_r\frac{d\eta_r(t)}{dt}, \end{aligned} \tag{1}$$

where $N(t)$ is the force applied to the beam, which is taken as zero in this paper since the beams undergo initial displacement leading to the beam's free vibrations response. Here, α_r and C_p are the electromechanical coupling term and capacitance of the beam respectively given by Equations (2) and (3):

$$C_p = \varepsilon_{33}^S\frac{w_p l_p}{t_p}, \tag{2}$$

$$\alpha_r = -Y_p d_{31} w_p t_{pc}\left.\frac{d\phi_r(x)}{dx}\right|_{x_1}^{x_2}, \tag{3}$$

where Y_p is the Young's modulus of the PE layer at constant electric field.

Table 2: Characteristics of the experimentally tested PVDF beams

Parameter	Beam	PVDF	Mylar	Units
L, W, T	$20, 13, 0.178$	$14.7, 10.2, 0.028$	$20, 13, 0.15$	mm
Beam's mass, m	6.72×10^{-5}	1.30×10^{-5}	5.42×10^{-5}	kg
Second moment, I	5.76×10^{-15}	-	-	m^4
Density, ρ	-	1780	1390	kg/m^3
Young modulus, E	4.41	2.7	5.0	GPa
Stiffness, k	9.53	-	-	N/m
PVDF constant, g_{31}	-	216×10^{-3}	-	Vm/N
PVDF constant, d_{31}	-	23	-	pC/N

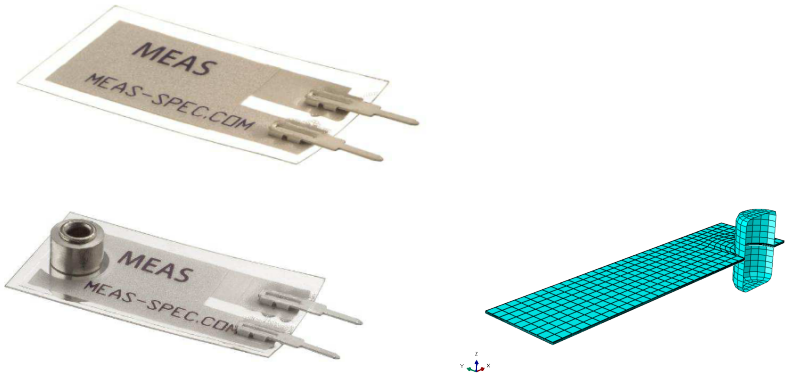

(a) (b)

Figure 4: (a) LDT0 and LDTM Beams [46] and (b) FEM model of the LDTM beam.

3.3. Finite element model

To ensure that the dynamic model describes well the beam's dynamics, first, a FEM model is developed. Since the beams' deformation pattern depends on the values of the overlap, a preliminary set of numerical simulations is conducted to identify the beam's stress as a function of the overlap. Figure 4a demonstrates the actual beams with and without mass, whereas Figure 4b presents the FE models of these beams created in Abaqus. The tip-mass beam is marked as LDTM, while the no mass beam is marked as LDT0. The explicit dynamic FE models developed to study the plectrum-beam interaction was composed of 312 linear quadrilateral shell elements for the LDT0 beam type while the LDTM type was composed of 448 linear quadrilateral shell elements and 192 linear triangular shell elements. The plectrum was modelled as a rigid body composed of 352 linear quadrilateral elements, moving under the gravity force.

The behaviour of both beams was simulated in Abaqus using an explicit analysis for different overlaps. It should be stressed that each beam is subjected to an initial displacement, corresponding to the geometry of the contact between the beam and the carriage's plectrum. Due to the geometrical features of the considered design, this initial displacement is completely defined by the geometrical dimensions of the beam, the plectrum, and the overlap. When contact is lost, the beam starts free vibrations due to the imposed deformation. Figure 5 demonstrates the normalised stress field in the PVDF layer imposed by a carriage's plectrum with different overlaps at the moment of the beam's maximum deformation. One

can observe, as expected, that the higher overlaps correspond to the higher attained maximum stresses in the beam, however, none of the them go beyond the yield stress of the material (45 MPa), reaching about 70 % of it for 10 mm overlap in the case of the massless beam. It should be stressed that although higher over-

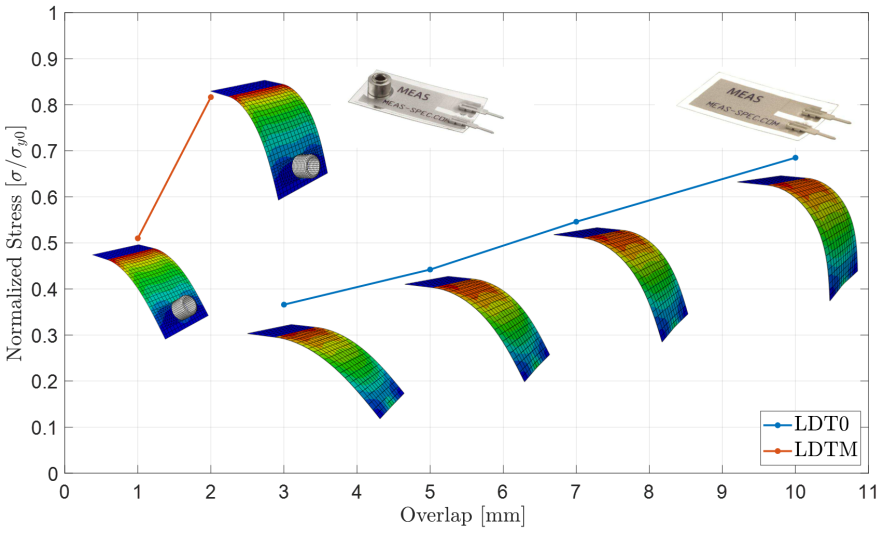

Figure 5: Stress field in both the tip-mass (LDTM) and the massless (LDT0) beams.

laps generate higher voltage, it is not ideal for the beams to undergo very large deflections from the fatigue/degradation point of view.

As expected, the tip-mass beam undergoes higher deformation for the same overlap due to the physical size of the mass, reaching over 80 % of the material's yield stress for 2 mm overlap. Indeed, because the lumped mass sticks out symmetrically from each side of the beam by 3 mm from the beam's surfaces, it becomes the main point of a contact with the moving mass, resulting in higher deformation compared to the massless beams. It was calculated in this case that the values of the overlap higher than 2 mm led to stresses which exceeded the yield stress, therefore these overlaps were not included in Figure 5.

3.4. Model Validation

The analysis is performed combining experimental, numerical and analytical procedures. First, an experimental procedure was performed using the PE beam connected to a non-optimal load. The electrical circuit, shown in Figure 6, is modelled in Matlab/Simulink according to the physical circuit used in the experiments.

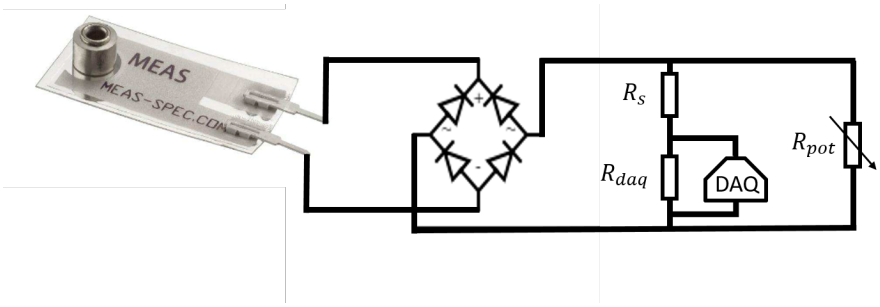

Figure 6: Energy harvester circuit used for the experimental procedures.

The circuit consists of a rectification bridge connected to the PVDF beam and to the Data Acquisition Card. The signal was recorded using LabView software over the R_{daq} resistor. The signal obtained experimentally provides information about the beam's natural frequency and damping coefficient ζ. For the numerical simulations, ζ was used to calculate the mass damping coefficient, which is $\alpha = 2\zeta\omega$.

Second, an explicit dynamic model is built in Abaqus to determine the maximum displacement experienced by the beams when impacted by a carriage's plectrum under several values of the overlaps. Third, the maximum displacement is adopted as the initial displacement η_0 and the free vibration response of the beam is obtained analytically. Lastly, having obtained the mechanical response of the beam, the output current is calculated and transmitted to MATLAB/Simulink as an input to the electrical circuit interface. Figure 7 presents a comparison of the numerical results obtained using the above developed semi-analytical model and experimental results for the massless and tip-mass beams. Overall, a good agreement between experimental and numerical voltage output with respect to the natural frequency and the damping ratio for the mass and massless beams is observed.

For a single or two opposite beams engaged and working simultaneously, the optimal load could be defined using the following formula for the steady state response [48]:

$$R_{opt} = \frac{\pi}{2C_p\omega}, \tag{4}$$

which assumes a standard PE circuit. Here C_p and ω are the capacitance and the natural frequency of the beam, respectively. Equation (4) then informs that for a given piezoelectric beam (i.e., for a given device capacitance Cp), the optimal resistance solely depends on the excitation frequency. Since the beam is plucked and freely vibrates at its first natural frequency, the optimal resistance is constant.

Therefore, for a single beam, the optimal resistance was around 14.7 $M\Omega$ as can be seen in Figure 8a. In the case when two beams are connected in parallel and vibrate simultaneously, the optimal resistance is around 7.4 $M\Omega$, which is half of value corresponding to the single beam, as shown in Figure 8b. The reason behind this reduction is related to the connection of two beams in parallel leading to doubled capacitance in the system. Figure 8 shows the numerical simulations results performed in Simulink, which agree well with the results yielded by (4). Reasonably good agreement with the experimental data can be found for both the beams thereby validating the developed numerical model for further use with multiple beams.

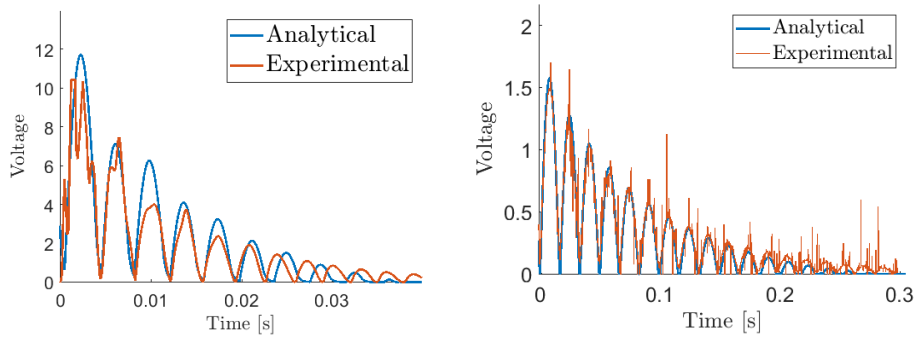

(a) Massless beam (b) Tip-mass beam.

Figure 7: Comparison between analytical and experimental voltage output for the (*a*) LDT0 beam and the (*b*) LDTM beam.

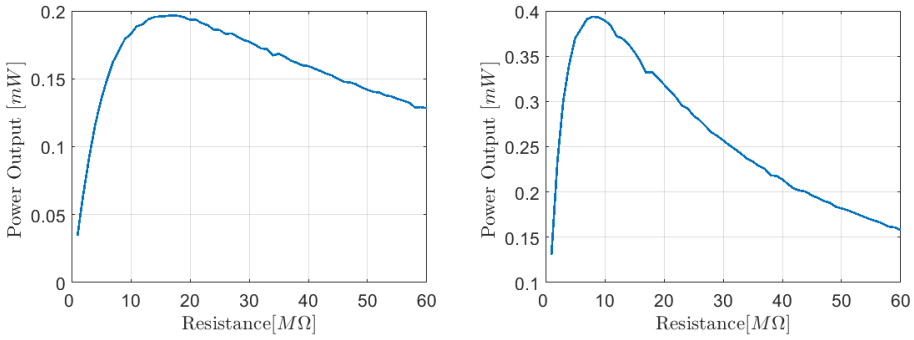

(a) (b)

Figure 8: Power generated by a (*a*) single beam and (*b*) 2 opposite beams engaged simultaneously.

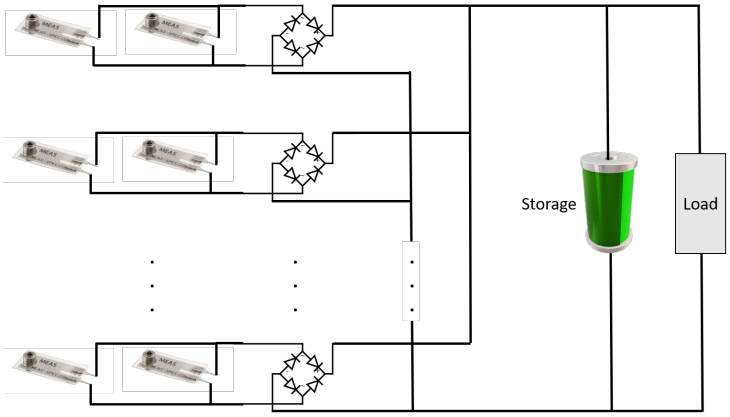

Figure 9: Energy harvester circuit with independent rectifiers and a smoothing capacitor.

3.5. Energy Harvesting Circuit

The developed and validated beam's model can be used to analyse the performance of several beams connected as a device. A straightforward mechanical consideration indicates that sufficient distance between the beams should be kept to avoid interaction or impacts of the beams against each other, while they are oscillating. There are also electrical issues to be taken into account. First of all, although all beams in this study have the dimensions, therefore the same natural frequency, they are naturally engaged at different time instances, leading to different phase shifts between the beams in the array. Secondly, the oscillation decay time in the system is higher than the time required for the mass to excite all beams. Thus, as can be seen in Figure 3, when the excitation of the last beam occurs, the first beam (the closest to the reader) in the array can still be under vibration.

All these factors lead to different instantaneous values of the response amplitude of each beam. As a whole, during each single run of the carriage, the beams produce a decaying harmonic signal shifted in time. Apart from pure mathematics, where such functions can be easily added, these electrical signals cannot be added unless they are either synchronised or converted to DC current, which in turn can be added according to the Kirchhoff's law. However, a typical AC-DC converter as shown in Figure 9 produces a constant DC current based on a constant amplitude harmonic input, whereas the signals from the beams are decaying and after rectification still cannot be considered as classical DC signals.

Therefore, a bridge rectifier, even when connected to a smoothing capacitor, is not capable of converting the beams' decaying output into DC. Another prob-

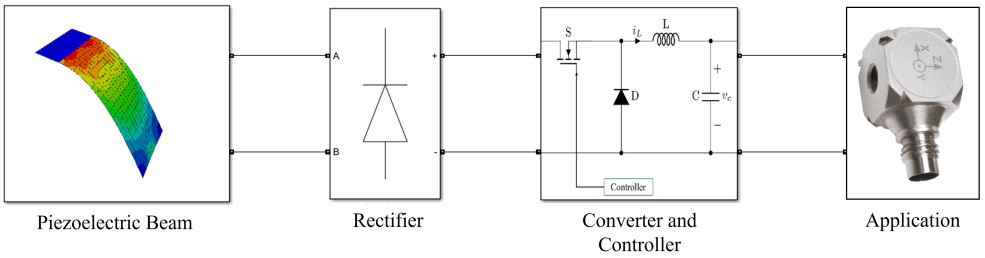

Figure 10: Energy harvester circuit proposed to minimize the charge cancellation from time-overlapping signals.

lem related to the decaying out-of-phase output generated by several beams is the charge cancellation issue, which decreases the total harvesting power. Lien and Shu [38] tried to address the charge cancellation problem by assigning an individual rectifier for each beam within the array and all rectifiers to a common smoothing capacitor and load, as illustrated in Figure 9. This approach, however, is inefficient since it will only avoid charging cancellation when all beams vibrate at the same frequency, with the same amplitude and in phase, which is clearly not the case here. If either of these parameters mismatch, charge cancellation will occur, e.g., when the output amplitude of a beam rises above that of other beams. Therefore, a power management circuit is necessary to extract the energy generated by the remaining oscillations from each beam and, thus, deliver a higher DC output.

Figure 10 shows the proposed energy harvester circuit to address the issues related to the decaying out-of-phase beams' output. It is composed of a bridge rectifier connected to a buck-boost DC-DC converter, which is then connected to a selected application. The main contribution and novelty in the proposed circuit is related to the strategy adopted in the operation of the controller of a DC-DC converter. In general terms, the duty cycle of the DC-DC converter is determined as a constant value given the input-output relationship. Given the operational conditions of the PE generator, this assumption is not valid as the circuit will operate in the transient condition on a permanent basis due to free vibrations of the beams, whereas the DC-DC's general relationship is obtained from the perspective that the bridge rectifier is sufficient to operate the AC-DC conversion. In fact, the buck-boost converter will not operate as a DC-DC converter but, in conjunction with the bridge rectifier, it will effectively operate as AC-DC converter.

It is obvious that most of the assumptions adopted for conventional energy

harvesting circuits in which a generator operates in the steady-state response cannot be applied to this application, that extends to any type of frequency-up based application. Instead of having the duty cycle defined in terms of the input-output ratio, the switch is controlled based on impedance tracking, yielding a varying duty cycle. In this context, the controller operates the switch in order to maintain the voltage across the capacitor at the optimal level for the maximum charge extraction. For a steady state operation, it is known that the power output of a PE generator is maximum when the voltage across the capacitor is half of the open-circuit voltage, which cannot be applied to our problem as the amplitude of the oscillation decays. Thus, defining the optimal voltage level across the smoothing capacitor is a critical decision, which will directly affect the effectiveness of the EH circuit.

3.6. Optimization Procedure

The optimisation procedure is carried out aided by the surrogate algorithm available in the optimisation toolbox provided by MATLAB. The surrogate algorithm receives this name due to the way the optimisation process is carried out, as it evaluates the surrogate of the objective function on several random points, where the surrogate is an approximation of the original function. This approach speeds up the evaluation process as the approximate model is constructed from the response obtained from a limited number of data points. The algorithm considers a function $E_T(\boldsymbol{p})$, which represents the total energy generated given the parameters $\boldsymbol{p}$. The parameters $\boldsymbol{p}$ is a input vector which may contain all the parameters to be optimised, e.g., the thickness of the piezoelectric layer, the thickness of the substrate layer, and the tip displacement of the beam, so that, $\boldsymbol{p} = [t_p,\, t_s,\, \delta]$. A objective function is defined as presented in (5):

$$\max_{\boldsymbol{p^i}} E_T(\boldsymbol{p^i}) \text{ when } b_{li} \leq \boldsymbol{p^i} \leq b_{ui} \tag{5}$$

where b_{li} and b_{ui} are the lower and upper bounds of the i^{th} parameter p^i. During the process, each set of suggested parameters $\boldsymbol{p}^i$ results into scalars E_T^i. This is a mapping process which can be expressed as $\{\boldsymbol{p}^i \rightarrow E_T^i = E_T(\boldsymbol{p}^i) | i = 1, 2, ..., n\}$ [49]. In this aspect, the surrogate algorithm carries out an iterative process which generates distinct designs given the leading parameters in the vector $\boldsymbol{p}$. It then evaluates the objective function and identify the inputs that more significantly impact the total energy output E_T. That is how the surrogate emulates the original objective function and replaces the expensive optimisation by another that is computationally cheaper to assess. Next, the maximum E_T value is selected. This

process is repeated until the distance between two points is less than the assigned tolerance.

4. Results of the optimisation

4.1. PVDF-based device

Since the produced power varies according to the beam's vibrations, a more appropriate measure is the amount of energy generated each time the beam is excited by the mass. The capacity of the capacitor has a direct effect on the amount of stored energy, which influence the rate of charging. The charging behaviour is dynamic and it depends not only on the capacitance used, but also on how long the latter will be charging before discharging and how long the cycle period is. For this reason, the energy harvester circuit must match the impedance of the PE beams to ensure optimal performance. An efficient way to match the impedance of the PE generator is to use a resistor connected in parallel and (4) can be used to define the optimal resistive load. The energy dissipated per beam array for a resistive load device (Figure 3a) is shown in Table 3 for different values of the inclination angles. Note that since the output is given per array and the device illustrated in Figure 3a is composed of two arrays, the total energy per device is doubled of that presented in Table 3. The surrogate optimisation algorithm was first applied to analyse the performance of the device with commercially available LDT0 and LDTM PVDF beams. The aim was to determine the optimum relationship between the number of the beams and displacement, given the constraints related to admissible stress, geometry, and inclination angle (see Table 3). When it comes to a single beam, Figure 11 presents the current (a) and charge (b) output of a single PVDF-LDTM beam after released from an initial displacement of 7.6 mm, which is the case for all simulations shown in Table 3. From Figure 11b, a charge density of 1.7 mC/m^2 is obtained per excitation.

A second analysis is run allowing the optimisation routine to determine the optimal substrate and PE material thickness, as presented in Table 4. In both tables, σ_{max} is the maximum stress achieved in the beam, θ is the device inclinations angle, M_{opt} is the minimal (Table 3) or the optimal carriage mass (Table 4) suggested by the numerical algorithm. The optimal mass is a function of the optimal carriage length l_{M-opt}, δ_b and n_b are the tip deflection and the overall number of beams correspondingly. The last three rows in the table are the total generated energy, E_T, in a single run, the time, $T/2$, required to complete the single run and the power density, $P_d = P_M/M_{opt}$, where $P_M = E_T/(T/2)$, which gives an

Table 3: Performance of the original unimorph beams device using surrogate optimisation.

	Device Configuration								Unit
	No Tip Mass				With Tip Mass				mm
θ	5°	15°	30°	45°	5°	15°	30°	45°	^{o}
σ_{max}	38.5	38.5	38.5	38.5	38.5	38.5	38.5	38.4	MPa
M_{opt}	0.157	0.053	0.027	0.019	0.157	0.053	0.027	0.019	kg
l_{M-opt}	17.6	5.92	3.06	2.17	17.6	5.92	3.06	2.17	mm
δ_b	7.6	7.6	7.6	7.6	7.6	7.6	7.6	7.6	mm
n_b	16	16	16	16	11	11	11	11	-
E_T	65	65	65	65	76	76	76	76	μJ
$T/2$	0.765	0.444	0.319	0.269	0.765	0.444	0.319	0.269	s
P_d	0.537	2.74	7.375	12.405	0.631	3.228	8.823	14.970	mW/kg

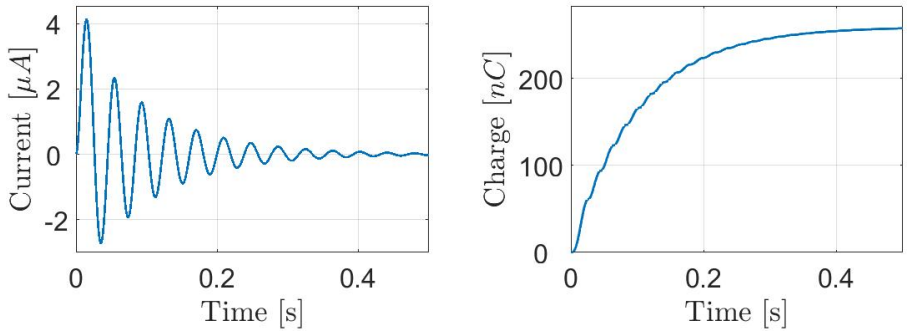

(a) (b)

Figure 11: Current (*a*) and Charge (*b*) generated by a single LDTM beam.

indication of the design efficiency. Note that the optimisation is carried at a predetermined inclination angle, which is constant throughout the procedure. The inclination angle is related to the device orientation, not to the beam orientation within the device. The beams are therefore always oriented at 90° with respect to the moving mass before they are excited. The thickness of the beam is an optimised parameter which uniformly changes for all beams within the device, so that they are all identical.

Assessing the results shown in Table 3, it can be deduced that the number of beams as well as the tip displacement did not vary across any of the inclination angles adopted. For this reason, there was no variation in the energy output response of the device. This occurred because the effective force provided by the mass at 5° is enough to impose the maximum admissible displacement that the beam is

able to experience, thus, increasing the effective force is of no use in this configuration. The power density, however, has improved, as it increases along with the inclination angle due to the higher effect of gravity, thereby lower mass needed to bend the beams, moreover, it requires less time to cover the distance from one end of the device to another. It can also be noted that larger displacement was preferable over the larger number of beams.

Table 3 also shows that the device's array can be composed of 16 LDT0 beams or 11 LDTM beams, which is due to the mass' height attached to the LDTM beam, since both beam types experience the same deflection. The device with the LDT0 beams generates about 65 μJ that is about 17 % lower than the energy generated by the device with the LDTM beams. Thus the device with the LDTM beams outperforms the one with the LDT0 beams even though the number of the beams is less by 5 than in the latter one. Since both LDT0 and LDTM beams undergo the same deflection, it can be concluded that, individually, the LDTM beams also have higher energy density than the LDT0 beams.

Table 4 presents a more robust optimisation case, where the thickness of the PE as well as the thickness of the substrate are optimised in addition to the tip displacement. In this table there are two extra rows of data, where t_{s-opt}, t_{p-opt} represent the optimal substrate thickness and the optimal PE material thickness respectively, achieved by the optimisation procedure. Note that with these considerations the number of the beams changes along with the device's inclination angle. Table 4 shows that the device with the LDTM beams no longer outperforms that composed of the LDT0 beams as the simulation procedure was able to make better use of the space available. In fact, the LDT0 device at 5° generates about 23 % more energy than the device with the LDTM beams, while being able to reach about 62 % more energy when operating at 30°. When compared to the original beam configuration outputs, shown in Table 3, Table 4 shows that the optimisation procedure was able to improve the device's performance 6.7-16.9 times when using the LDT0 beams and 4.6-9.8 times when using the LDTM beams, depending on the operation angle.

For the doubled array device, the voltage across the load is the same as that of the single-array device, however, the current in the circuit is doubled since the beams in the opposite array are connected in parallel (see Figure 9). Connecting the PE device to a purely resistive load, however, is limited in several ways from a practical point of view, e.g., most devices requires a DC source to operate. For this reason, the Standard Energy Harvesting (SEH) circuit is adopted for its versatility and easy implementation, as shown in Figure 9. In this circuit, each pair of the beams is connected to a full bridge rectifier, and each rectifier is connected to a

Table 4: Optimised performance based on optimum displacement, piezoelectric and substrate thickness using surrogate optimisation.

	Device Configuration								Unit
	No Tip Mass				With Tip Mass				mm
θ	5°	15°	30°	45°	5°	15°	30°	45°	^{o}
σ_{max}	36.2	37.3	38.10	37.52	38.1	38.4	38.4	38.4	MPa
M_{opt}	1.113	0.581	0.354	0.271	1.166	0.694	0.647	0.314	kg
l_{M-opt}	124.4	64.9	39.6	30.3	130.3	77.6	72.3	35.1	mm
t_{s-opt}	315	439	485	521	307	486	720	564	μm
t_{p-opt}	223	200	194	185	232	195	154	180	μm
δ_b	2.23	2.0	1.94	1.84	2.32	1.95	1.53	1.80	mm
n_b	27	42	48	52	12	17	18	20	-
E_T	433	845	1041	1097	352	628	642	748	μJ
$T/2$	0.765	0.444	0.319	0.269	0.765	0.444	0.319	0.269	s
P_d	0.508	3.27	9.20	15.04	0.394	2.035	3.110	8.854	mW/kg

common smoothing capacitor, as suggested by [38].

The power response from a single original-beam array, i.e., from 16 beams with their original thickness, is presented in Figure 12 for various inclination angles of the device using the SEH circuit. The supplementary four zoom-in figures demonstrate the charging/discharging stages for each angle studied. It can be seen that the peak to through height is almost identical to all inclination angles and is about 7-8μW, however, the period of the signals is reduced when the angle increases. When comparing the average power output given by Figure 12 through the SEH circuit against the $P_R = E_T/(T/2)$ shown in Table 4, which was calculated for a pure resistive load, it is clear that some energy is lost in the process, as expected. The ratio P_{SEH}/P_R is 34/85 (40.0%) for 5°, 66.9/146.4 (46.4%) for 15°, 99.3/203.8 (45.7%) for 30°, and 124.4/241.6 (51.5%) for 45°.

There are mainly two reasons for that discrepancy: the decaying nature of free vibrations and the time-overlapped signals. Due to the free vibrations, the signal generated by the beam, even after rectification, is decaying in time. The problem is that the smoothing capacitor operates at an optimal voltage. In normal circumstances, i.e., having non-decaying sinusoidal signals, the voltage level would be always equal to half of the open circuit voltage $V_{oc}/2$ generated by the beam. Although the voltage value is being changed in the current device, there is a voltage level around $V_{oc}/2$ at which the capacitor allows the optimal power extraction, which is tuned through the resistor in parallel. This means that all charges gener-

ated by the beams below the capacitor's voltage level will be wasted, i.e., charges generated initially under higher amplitudes will get through but once the voltage decays to the capacitor's level, the charge's flow stops.

The other issue, related to the time-overlapped signals, is better understood by examination of Figure 13, which illustrates how the device operates when each beam is connected to a bridge rectifier. Once the device is inclined, the carriage moves under the action of gravity toward the beams. Then, it plucks through all the beams with increasing velocity until reaching the opposite end of the device. As the velocity of the carriage increases, the time between beams' engagements reduces. However, as shown in Figure 13 and as explained in Section 3.5, the SEH circuit configuration with independent rectifier does not eliminate the charge cancellation if the a previous beam is still vibrating while the subsequent beam is excited. Figure 13 illustrates well this issue: going from right to left, note that Beam 1 first vibrates about 1.5 per cycles or reaches 3 peaks, which is related to the time ($t_{b1}^{\rightleftharpoons}$) that the mass took to first pluck it, come to a full stop, and then pluck it again on its way back. Within this time frame, the signal of Beam 1 is interrupted by itself as it is excited again. However, as Beam 2 is plucked, the signal from Beam 1 is interrupted after about only one cycle, even though it is still vibrating and thus capable of generating some charge. As the mass's velocity increases due to gravity, the time between pluckings is reduced, e.g., the signal generated by Beam 8 is interrupted long before it is able to complete its half-cycle.

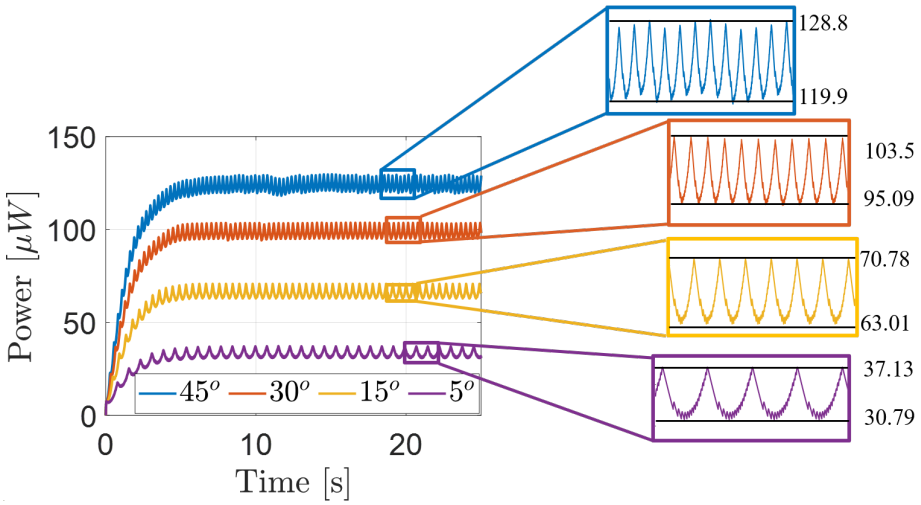

Figure 12: Power Output from the 16-beam array under the SEH circuit configuration at various angles.

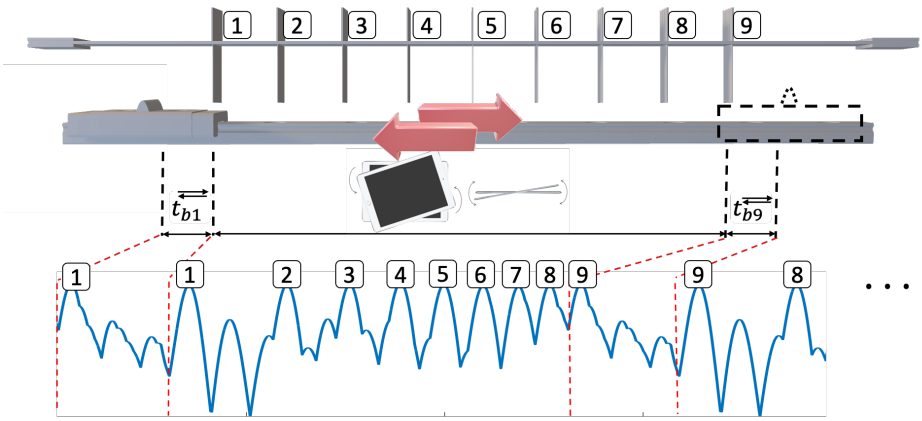

Figure 13: Device Operation

The interrupted signal points to the fact that the electrical power generated in the remaining oscillations are lost due to the rectification connection to a common smoothing capacitor.

The Energy Harvesting Circuit proposed in Section 3.5 addresses the second limitation. In the proposed configuration, the time-overlap issue is solved by adding a DC-DC converter in addition to the rectification bridge. However, the controller is the key for efficiency as it maintains the smoothing capacitor at the optimal voltage level to allow optimal charge extraction. The advantage of the proposed circuit is more prominent when there are more signals overlapping. In the case where no signal overlaps, the proposed circuit will behave like the SEH circuit. Comparing the device with the original LDT0 beams under both circuits, the proposed circuit was able to improve the efficiency from 40 % to 75% for the case where the device was inclined at 5°.

4.2. Health monitoring of wind turbine blades

The number of onshore and offshore wind farms and solitary wind turbines has been rapidly growing in the last two decades. Modern wind turbines can be over 150 meters toll, with blades as long as 100 meters. The blades play the key role in renewable wind energy, therefore their structural health monitoring is one of the important issues. Inspections and maintenance of the blades contribute significantly towards the overall cost of generated electricity. Thus, various technologies and numerous approaches have been developed for the identification of various types of damage to the blades [50]. Some of the them rely on wireless sensors, which can be installed inside the blades within their first 1/3-length from

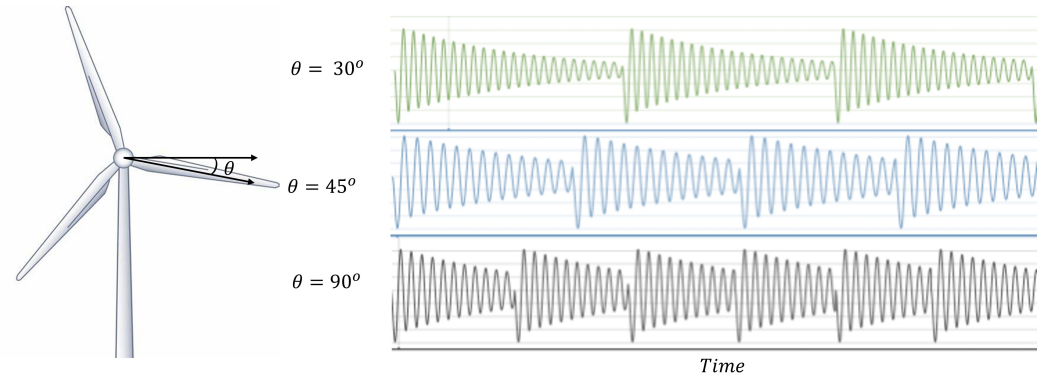

Figure 14: Response of the beams as the mass slides due to the gravity force as the blade rotates.

the hub. The larger the number of sensors the better and more reliable the assessment of the blades' structural health, thereby the better and easier the decision making process regarding operating and maintenance of the wind turbines. However, these wireless sensors require some power to operate and transmit data to the operators. To power health monitoring sensors, the proposed EH device can be used, placed inside and along a blade as shown in Figure 15 left, so that the device's mass will slight down every time the blade is in the vertical position (twice per revolution). For the device to operate it is essential that the centripetal force acting on the carriage does not exceed the gravity force, $g > \omega^2(L+r)$, where ω is the angular speed of the blade, L is the device length and r is the absolute distance to the device from the rotational axis. This inequality provides a restriction to the device size and/or place of the device within the blade. Figure 14 illustrates the response of sequential beams as the mass slides on the rails plucking the beams.

Using the proposed methodology the power density of 3 devices will be compared first. The first device will comprise a mass with a single plectrum and PVDF LDT0 beams, whereas the second device will be similar to the first one but it has a multiple plectra attached to the carriage, which will be optimised. The third device will also have multiple plectra attached to the carriage but utilizes $LiNbO_3$ beams. All the devices were taken to be 1 m long. The optimisation yielded 5 mJ for the first configuration, 128 mJ for the second, and 563 mJ for the third device respectively. As the results indicate, there is a substantial increase of 25.6 times in the energy output by implementing the multiple plectra technique proposed in [39]. Since much lower deflection of $LiNbO_3$ beams (around 50 times lower than in PVDF) can produce more or less the same voltage and power output, the number of beams per unit length in the $LiNbO_3$-based device grows significantly,

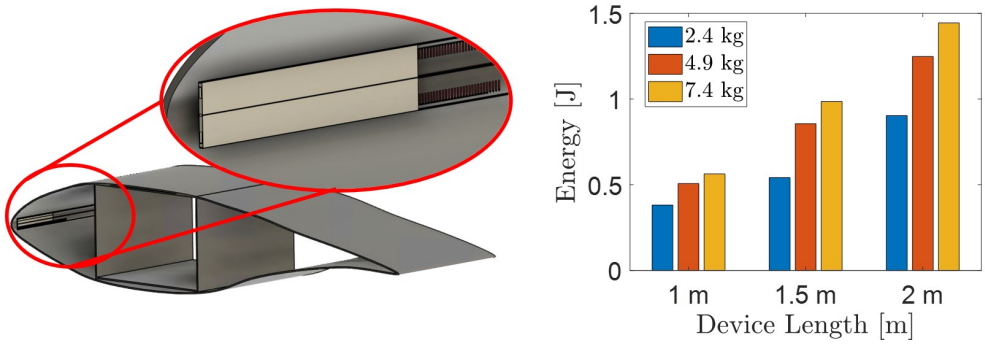

Figure 15: Energy output for the device under 3 lengths and carriage masses when harvesting energy from the blade rotation.

increasing the power density of the device. Obviously, such a device can produce several orders of magnitude higher energy output than that based on PVDF beams.

Figure 15 (right) presents the energy output for the $LiNbO_3$ device with 3 different lengths and carriage masses configurations when harvesting energy inside the blade. The proposed optimisation approach has indicated that 7.4 kg optimal device consisted of 830, 1339, and 1824 beams of 20x5x0.63 mm^3, 20x5x0.67 mm^3, and 20x5x0.69 mm^3 size correspondingly. It can be observed that all devices produce a significant amount of power, moreover, the power increase is higher than linear when the device length is increased. Indeed, increasing the device length twice leads to almost a threefold increase in the harvested energy. Moreover, the optimisation algorithm effectively selected the optimal thickness of the beams and the overall number of excitations, leading to 0.5-1.0 W in the case of 2-meter long device, depending on the rotational speed of the blades, which varies for large turbines between 10 and 30 rpm. The device is able to reach a power density of 1.06 mW/cm^3, which is several times or an order of magnitude higher than the power density provided by other EH in the same application field [51, 52, 53, 54, 55].

5. Conclusions

This paper proposes a new optimisation methodology for developing high-power vibration EH device based on piezoelectric cantilever beams and gravity-driven motion of a bulk carriage. The proposed device's layout has a comb-like structure and can be scaled up or down based on the dimensions of a targeted host. The device's operating principle is based on the sliding motion of the car-

riage mass, which plucks the beams, providing them with an initial displacement, launching the beams' free vibrations. Two different types of beams have been investigated: flexible PVDF beams and much stiffer $LiNbO_3$ beams. The experiments conducted with PVDF beams validated the finite element model and numerical dynamic model of the concept. These models have then been used to study the device's performance when the beams either have or not tip mass.

The optimisation procedure, applied to the PVDF-based device, took into account only the space occupied by the beams in the competing decision about increasing their tip displacement or adding more beams, given an inclination angle and required carriage mass. The outcome of this stage yielded similar results as the device generated the same amount of energy across all inclinations angles. Clearly, higher inclinations angles requires lower carriage mass and allows generating the same amount of energy in a shorter time. Thus, the power density has increased for higher inclination angles, although the energy output remained the same. Important to note that the device composed of the LDTM (with tip-mass) beams generated about 17 % higher energy output than the device composed of the LDT0 (without tip mass) beams, even though the last one had more beams. Furthermore, the proposed algorithm optimised not only the space occupied by the beams but also their substrate and piezoelectric material thicknesses. Through this procedure, the device's performance increased between 6.7 and 16.9 times when using the LDT0 beams and between 4.6 and 9.8 times when using the LDTM beams, depending on the operation angle. It allowed the device with the LDT0 beams to outperform the device with the LDTM beams, however, to accomplish this result, the obtained substrate layer was between 2 and 3.8 times thicker and the piezoelectric layer was about 5.5 to 8.3 thicker than the original ones. This led to substantial increase in the beam's stiffness, consequently increasing the required carriage mass to pluck it. Therefore, even though the power performance has increased substantially, the overall power density remained at the same level.

The SEH circuit was integrated with the device layout considering the out-of-phase and decaying free vibration response of the beams. Even though the beams are always operating in the free-vibration state, the proposed device has been able to operate at 0.68 Hz (5° inclination angle) and it has been sufficient to reach a steady state power generation. The 32 beams device, having 16 beams at each side, at 5° was able to deliver about 68 μW at a constant rate when the smoothing capacitor has reached steady state. It was also discussed that a lot of the charge generated is wasted due to overlapping signals in time, for which a new circuit, capable of resolving this issue and increasing the device's efficiency, has been proposed. Using the same device at 5° with the new circuit has increased

the power output from 68 μW to 150 μW, resulting an increase of 88% in power output, which caused the efficiency to improve by 35% reaching 75% of efficiency when compared to the energy dissipated across a pure resistive load.

The proposed optimisation methodology was applied to PVDF - based and $LiNbO_3$ - based beams to compare their performance to power wireless sensors and data transmission unit for wind turbines blade health monitoring application. It has been demonstrated that stiff $LiNbO_3$ beams with multiple plucking have substantially outperformed PVDF beams, thus the former were used to create a potential EH device for internal wind blades wireless sensors. It has been demonstrated that a 1-2 meter long device, which can be placed along the blade's length near the hub, can generate from 0.5-1.5 J, and depending on the rotational speed of the blades it results in power of 0.5 to 1 W, reaching a power density of 1.06 mW/cm^3.

Acknowledgments

The authors would like to acknowledge and are thankful for the support received from the Brazilian National Council for Scientific and Technological Development—CNPq, grant 202615/2019-7.

Limitation of Study

The authors acknowledge that the beam-plectrum interaction may lead to disturbances in the signal, which is not considered in the optimisation procedure. However, the interaction takes place for a short period of time and the energy accounted for in the simulation is mainly from the free vibration after release. In addition, the experimental results demonstrate that, despite the complex dynamics involved in the impact, the beam continues to vibrate at its first natural frequency, as expected.

References

[1] G. Clementi, G. Lombardi, S. Margueron, M. A. Suarez, E. Lebrasseur, S. Ballandras, J. Imbaud, F. Lardet-Vieudrin, L. Gauthier-Manuel, B. Dulmet, M. Lallart, A. Bartasyte, Linbo$_3$ films – a low-cost alternative lead-free piezoelectric material for vibrational energy harvesters, Mechanical Systems and Signal Processing 149 (2021).

[2] E. Sisinni, A. Saifullah, S. Han, U. Jennehag, M. Gidlund, Industrial internet of things: Challenges, opportunities, and directions, IEEE Transactions on Industrial Informatics 14 (11) (2018) 4724–4734.

[3] M. Gorlatova, J. Sarik, G. Grebla, M. Cong, I. Kymissis, G. Zussman, Movers and shakers: Kinetic energy harvesting for the internet of things, SIGMETRICS Perform. Eval. Rev. 42 (1) (2014) 407–419.

[4] J. Siang, M. Lim, M. Salman Leong, Review of vibration-based energy harvesting technology: Mechanism and architectural approach, International Journal of Energy Research 42 (5) (2018) 1866–1893.

[5] C. Gould, R. Edwards, Review on micro-energy harvesting technologies, in: 2016 51st International Universities Power Engineering Conference (UPEC), 2016, pp. 1–5.

[6] M. Hendijanizadeh, S. M. Sharkh, M. Moshrefi-Torbati, Energy harvesting from a rotational transducer under random excitation, JOURNAL OF RENEWABLE AND SUSTAINABLE ENERGY (2014).

[7] Z. Yang, S. Zhou, J. Zu, D. Inman, High-performance piezoelectric energy harvesters and their applications, Joule 2 (4) (2018) 642–697.

[8] S. Roy, D. Mallick, K. Paul, Mems-based vibrational energy harvesting and conversion employing micro-/nano-magnetics, IEEE Transactions on Magnetics 55 (7) (2019) 1–15.

[9] G. Thomson, D. Yurchenko, D. V. Val, Dielectric elastomers for energy harvesting, in: R. Manyala (Ed.), Energy Harvesting, IntechOpen, 2018, Ch. 4, pp. 41–61.

[10] I. Collins, M. Hossain, W. Dettmer, I. Masters, Flexible membrane structures for wave energy harvesting: A review of the developments, materials and computational modelling approaches, Renewable and Sustainable Energy Reviews 151 (2021) 111478.

[11] D. Barkas, C. Psomopoulos, P. Papageorgas, K. Kalkanis, D. Piromalis, A. Mouratidis, Sustainable energy harvesting through triboelectric nano – generators: A review of current status and applications, Energy Procedia 157 (2019) 999 – 1010.

[12] G.-J. Lee, M.-K. Lee, J.-J. Park, D. Y. Hyeon, C. K. Jeong, K.-I. Park, Piezoelectric energy harvesting from two-dimensional boron nitride nanoflakes, ACS Applied Materials & Interfaces 11 (41) (2019) 37920–37926. doi:10.1021/acsami.9b12187.

[13] J. Wang, L. Geng, L. Ding, H. Zhu, D. Yurchenko, The state-of-the-art review on energy harvesting from flow-induced vibrations, Applied Energy 267 (2020).

[14] J. Wang, D. Yurchenko, G. Hu, L. Zhao, L. Tang, Y. Yang, Perspectives in flow-induced vibration energy harvesting, Applied Physics Letters 119 (10) (2021) 100502. doi:10.1063/5.0063488.

[15] H. Fu, E. M. Yeatman, A methodology for low-speed broadband rotational energy harvesting using piezoelectric transduction and frequency up-conversion, Energy 125 (2017) 152–161.

[16] X. Mei, S. Zhou, Z. Yang, T. Kaizuka, K. Nakano, The benefits of an asymmetric tri-stable energy harvester in low-frequency rotational motion, Applied Physics Express 12 (5) (2019).

[17] H. Fu, X. Mei, D. Yurchenko, S. Zhou, S. Theodossiades, K. Nakano, E. M. Yeatman, Rotational energy harvesting for self-powered sensing, Joule 5 (5) (2021) 1074–1118. doi:https://doi.org/10.1016/j.joule.2021.03.006.

[18] D. F. Wang, Y. Zhu, X. Yang, C. Xia, Y. Fu, J. Song, A ball-impact piezoelectric converter wrapped by copper coils, IEEE Transactions on Nanotechnology 17 (4) (2018) 723–726.

[19] G. Martínez Ayuso, M. Friswell, S. Adhikari, H. Khodaparast, C. Featherston, Energy harvesting using porous piezoelectric beam with impacts, Procedia Engineering 199 (2017) 3468–3473.

[20] N. Yan, A. Basari, K. Leong, N. Nawir, Piezoelectric energy harvesting system via impact and vibration – a review, Journal of Telecommunication, Electronic and Computer Engineering 11 (2019) 35–41.

[21] K. Meruane, V.; Pichara, A broadband vibration-based energy harvester using an array of piezoelectric beams connected by springs, Shock and Vibration (2016).

[22] H. Liu, C. Quan, C. J. Tay, T. Kobayashi, C. Lee, A mems-based piezoelectric cantilever patterned with pzt thin film array for harvesting energy from low frequency vibrations, Physics Procedia 19 (2011) 129–133, international Conference on Optics in Precision Engineering and Nanotechnology (ICOPEN 2011). doi:https://doi.org/10.1016/j.phpro.2011.06.136.

[23] T. Kim, Y. Ko, C. Yoo, B. Choi, S. Han, N. Kim, Design optimisation of wide-band piezoelectric energy harvesters for self-powered devices, Energy Conversion and Management 225 (2020) 113443. doi:https://doi.org/10.1016/j.enconman.2020.113443.

[24] N. Chen, H. J. Jung, H. Jabbar, T. H. Sung, T. Wei, A piezoelectric impact-induced vibration cantilever energy harvester from speed bump with a low-power power management circuit, Sensors and Actuators A: Physical 254 (2017) 134–144.

[25] A. Abedini, F. Wang, Energy harvesting of a frequency up-conversion piezoelectric harvester with controlled impact, The European Physical Journal Special Topics 228 (6) (2019) 1459–1474.

[26] R. Dauksevicius, R. Gaidys, V. Ostasevicius, R. Lockhart, A. V. Quintero, N. de Rooij, D. Briand, Nonlinear piezoelectric vibration energy harvester with frequency-tuned impacting resonators for improving broadband performance at low frequencies, Smart Materials and Structures 28 (2) (jan 2019).

[27] X. Rui, Y. Zhang, Z. Zeng, G. Yue, X. Huang, J. Li, Design and analysis of a broadband three-beam impact piezoelectric energy harvester for low-frequency rotational motion, Mechanical Systems and Signal Processing 149 (2021).

[28] B. Kathpalia, D. Tan, I. Stern, A. Erturk, An experimentally validated model for geometrically nonlinear plucking-based frequency up-conversion in energy harvesting, Smart Materials and Structures 27 (1) (dec 2017).

[29] Y. Kuang, M. Zhu, Design study of a mechanically plucked piezoelectric energy harvester using validated finite element modelling, Sensors and Actuators A: Physical 263 (2017) 510–520.

[30] Z. Chen, F. Zhang, X. Xu, Z. Chen, W. Li, F. Li, J. Han, H. Zhou, K. Xu, L. Bu, Non-contact multiple plucking method for frequency up conver-

sion piezoelectric energy harvesters in extremely low frequency applications, in: 2019 20th International Conference on Solid-State Sensors, Actuators and Microsystems Eurosensors XXXIII (TRANSDUCERS EUROSENSORS XXXIII), 2019, pp. 1427–1430.

[31] Y. Kuang, Z. Yang, M. Zhu, Design and characterisation of a piezoelectric knee-joint energy harvester with frequency up-conversion through magnetic plucking, Smart Materials and Structures 25 (8) (jul 2016).

[32] T. Xue, S. Roundy, On magnetic plucking configurations for frequency up-converting mechanical energy harvesters, Sensors and Actuators A: Physical 253 (2017) 101–111.

[33] Y. Wu, J. Qiu, F. Kojima, H. Ji, W. Xie, S. Zhou, Design methodology of a frequency up-converting energy harvester based on dual-cantilever and pendulum structures, AIP Advances 9 (4) (2019).

[34] L. Gu, C. Livermore, Impact-driven, frequency up-converting coupled vibration energy harvesting device for low frequency operation, Smart Materials and Structures 20 (4) (2011).

[35] P. Peralta, R. Ruiz, S. Natarajan, E. Atroshchenko, Parametric study and shape optimization of piezoelectric energy harvesters by isogeometric analysis and kriging metamodeling, Journal of Sound and Vibration 484 (2020).

[36] A. A. Hashim, K. I. Mahmoud, H. M. Ridha, Geometry and shape optimization of piezoelectric cantilever energy harvester using comsol multiphysics software, International Review of Applied Sciences and Engineering IRASE (04 Mar. 2021).

[37] I. C. Lien, Y. C. Shu, Array of piezoelectric energy harvesting by the equivalent impedance approach, Smart Materials and Structures 21 (8) (2012).

[38] I. C. Lien, Y. C. Shu, Piezoelectric array of oscillators with respective electrical rectification, in: H. Sodano (Ed.), Active and Passive Smart Structures and Integrated Systems 2013, Vol. 8688, International Society for Optics and Photonics, SPIE, 2013, pp. 25 – 32.

[39] L. Q. Machado, D. Yurchenko, J. Wang, G. Clementi, S. Margueron, A. Bartasyte, Multi-dimensional constrained energy optimization

of a piezoelectric harvester for e-gadgets, iScience 24 (7) (Jul 2021). doi:10.1016/j.isci.2021.102749.

[40] M. Pozzi, Synchronicity and pure bending of bimorphs: a new approach to piezoelectric energy harvesting 27 (8) (2018) 085027. doi:10.1088/1361-665x/aad073.
URL https://doi.org/10.1088/1361-665x/aad073

[41] L. Dong, C. Wen, Y. Liu, Z. Xu, A. B. Closson, X. Han, G. P. Escobar, M. Oglesby, M. Feldman, Z. Chen, J. X. J. Zhang, Piezoelectric buckled beam array on a pacemaker lead for energy harvesting, Advanced Materials Technologies 4 (1) (2019).

[42] B. Y. Jing, K. S. Leong, Power optimization configuration for piezoelectric cantilever arrays, MATEC Web Conf. (2017).

[43] I. C. Lien, Y. C. Shu, Array of piezoelectric energy harvesters, in: M. N. Ghasemi-Nejhad (Ed.), Active and Passive Smart Structures and Integrated Systems 2011, Vol. 7977, International Society for Optics and Photonics, SPIE, 2011, pp. 215 – 223.

[44] S. Mishra, L. Unnikrishnan, S. K. Nayak, S. Mohanty, Advances in piezoelectric polymer composites for energy harvesting applications: A systematic review, Macromolecular Materials and Engineering 304 (1) (2019) 1800463.

[45] C. K. Jeong, D. Y. Hyeon, G.-T. Hwang, G.-J. Lee, M.-K. Lee, J.-J. Park, K.-I. Park, Nanowire-percolated piezoelectric copolymer-based highly transparent and flexible self-powered sensors, J. Mater. Chem. A 7 (2019) 25481–25489. doi:10.1039/C9TA09864J.

[46] I. Measurement Specialties, Ldt with crimps vibration sensor/switch, Measurement Specialties, Inc. (2008).

[47] A. Erturk, D. J. Inman, A Distributed Parameter Electromechanical Model for Cantilevered Piezoelectric Energy Harvesters, Journal of Vibration and Acoustics 130 (4) (2008).

[48] W.-J. Wu, A. M. Wickenheiser, T. Reissman, E. Garcia, Modeling and experimental verification of synchronized discharging techniques for boosting

power harvesting from piezoelectric transducers, Smart Materials and Structures 18 (2009) 055012.

[49] A. Forrester, A. Sóbester, A. Keane, Constructing a Surrogate, John Wiley & Sons, Ltd, 2008, Ch. 2, pp. 33–76.

[50] Y. Du, S. Zhou, X. Jing, Y. Peng, H. Wu, N. Kwok, Damage detection techniques for wind turbine blades: A review, Mechanical Systems and Signal Processing 141 (2020) 106445.

[51] C. L. Zhang, Z. H. Lai, G. Q. Zhang, D. Yurchenko, Energy harvesting from a dynamic vibro-impact dielectric elastomer generator subjected to rotational excitations, Nonlinear Dynamics 102 (3) (2020) 1271–1284.

[52] C. L. Zhang, Z. H. Lai, M. Q. Li, D. Yurchenko, Wind energy harvesting from a conventional turbine structure with an embedded vibro-impact dielectric elastomer generator, Journal of Sound and Vibration 487 (2020) 115616.

[53] Y. Zhang, R. Zheng, K. Shimono, T. Kaizuka, K. Nakano, Effectiveness testing of a piezoelectric energy harvester for an automobile wheel using stochastic resonance, Sensors 16 (10) (2016) 1727. doi:10.3390/s16101727.
URL https://doi.org/10.3390/s16101727

[54] Y.-Y. Feng, S.-J. Chen, S.-P. Cheng, Development of a miniaturized rotational electromagnetic energy harvester with a liquid metal direct-write process, Sensors and Actuators A: Physical 295 (2019) 224–230. doi:10.1016/j.sna.2019.05.001.
URL https://doi.org/10.1016/j.sna.2019.05.001

[55] W. Sun, F. Guo, J. Seok, Development of a novel vibro-wind galloping energy harvester with high power density incorporated with a nested bluff-body structure, Energy Conversion and Management 197 (2019) 111880. doi:10.1016/j.enconman.2019.111880.